Optimization of EBSD parameters for ultra-fast characterization

Y. CHEN, J. HJELEN, S.S. GIREESH & H.J. ROVEN
Norwegian University of Science and Technology (NTNU), Department of Materials Science and Engineering, Trondheim, Norway

Key words. Contamination, effective spatial resolution, electron backscatter diffraction (EBSD), probe current, step size, ultrafine-grained materials.

Summary

Ultra-fast pattern acquisition of electron backscatter diffraction and offline indexing could become a dominant technique over online electron backscatter diffraction to investigate the microstructures of a wide range of materials, especially for *in situ* experiments or very large scans. However, less attention has been paid to optimize the parameters related to ultra-fast electron backscatter diffraction. The present results show that contamination on a clean and unmounted specimen is not a problem even at step sizes as small as 1 nm at a vacuum degree of 6.1×10^{-5} Pa. There exists an optimum step size at about 50 data acquisition board units. A new and easy method to calculate the effective spatial resolution is proposed. Effective spatial resolution tends to increase slightly as the probe current increases from 10 to 100 nA. The fraction of indexed points decreases slightly as the frame rate increases from 128 patterns per second (pps) to 835 pps by compensating the probe current at the same ratio. The value 96 × 96 is found to be the optimum pattern resolution to obtain optimum speed and image quality. For a fixed position of electron backscatter diffraction detector, the fraction of indexed points as a function of working distance has a maximum value and drops sharply by shortening the working distance and it decreases slowly with increasing the working distance.

Introduction

Electron backscatter diffraction (EBSD)/electron backscatter patterns (EBSP) is a powerful technique to automatically and quantitatively measure the orientation of grains and phases of a wide range of materials, e.g. metals (Chen *et al.*, 2010), minerals (Magdalena, 2003), ceramics (Koblischka-Veneva *et al.*, 2002) and semiconductor (Chen *et al.*, 2005). With the rapid development of bulk nanostructured materials or ultrafine-grained materials fabricated by severe plastic deformation (Valiev *et al.*, 2000), there has been a growing interest of investigating grain and subgrain size, texture (Schwartz *et al.*, 2000), local deformation (Geiss *et al.*, 2005), dislocation density (Pantleon, 2008), stored energy (Saxl *et al.*, 2009) and strain analysis (Wright *et al.*, 2011). At the same time, investigation of heavily deformed materials by EBSD will be a challenge on both a very fine grain size (nanoscale) and the poor pattern quality associated with nanostructured / ultrafine-grained materials.

The term of EBSP was proposed when the phosphor screen and the TV camera were first used to record the patterns (Venables & Harland, 1973). Since then, the EBSD technique has experienced two important steps. Step 1, reliable automatic indexing (Krieger Lassen *et al.*, 1992), Step 2, ultra-fast speed based on offline EBSD collection and re-indexing techniques (EDAX/TSL, 2007; Søfferud *et al.*, 2007, 2008a, b) assisted by improvements in digital camera and modern computer (Wright & Nowell, 2008). The offline EBSD technique adopts the idea of separating the acquisition and indexing processes to take many advantages over online EBSD (Schwarzer & Hjelen, 2010). With the increasing acquisition speed, the quality of the patterns acquired at ultra-fast speed becomes the main concern (Nowell *et al.*, 2003; Maitland, 2004), especially for the heavily deformed materials. Moreover, many parameters like contamination, step size, probe current and pattern resolution are important to be optimized. However, there are few studies on the quantification of patterns acquired at ultra-fast speed and optimization of the parameters related to ultra-fast EBSP performance. The aim of this study is to optimize the EBSD parameters at high acquisition speed based on both coarse- and fine-grained materials.

Materials and methods

Two grade 2 commercial pure titanium (Ti) samples, coarse- and fine-grained microstructures, were used in this study. The

Correspondence to: Dr Yongjun Chen, Department of Materials Science and Engineering, Norwegian University of Science and Technology (NTNU), Alfred Getz vei 2b, 7491 Trondheim, Norway. Tel.: +47-73594921; Fax: +47-73590203; e-mail: happywinner01@gmail.com

coarse-grained Ti sample with average grain size of 25μm was used in rolled and annealed condition. The fine grained Ti sample with average grain size `of about 0.5 μm was used in the condition of equal channel angular pressing (ECAP) 4 passes (Chen *et al.*, 2011). The microstructure of coarse- grained Ti is fully recrystallized and equiaxed whereas the fine-grained Ti has slightly elongated grains and a lot of strain and residual stress at grain boundaries due to heavy deformation.

Samples for the EBSD study were prepared by mechanical grinding, mechanical polishing and final electropolishing with a Struers A3 solution (Ballerup, Denmark), using a voltage of 40 V for 15–25 s under a controlled temperature of –30˚C. The samples were cleaned with methanol and finally cleaned 5 min in a Fischione (PA, USA) plasma cleaner (model 1020). The EBSD collection was done in a Zeiss Ultra 55 FEGSEM (Oberkochen, Germany). The patterns were acquired and streamed to hard disk by a NORDIF UF-1000 EBSD detector (www.nordif.com; Trondheim, Norway). For patterns offline indexing and data analysis, EDAX/TSL OIM 5.3 software was used. In order to obtain universal and statistical results, the term of 'indexed points' is adopted to reveal the indexing rate, which is linked to pattern intensity and quality. The indexed points mean the fraction of points with a confidence index (CI) higher than 0.08 and all results concerning the error bar of indexed points are obtained from the average of three maps from different areas. The actual probe current was measured with a Faraday cup. The samples were tilted 70˚ for EBSD mapping for all experiments. The accelerating voltage was 20 kV and the working distance was around 20 mm except for the last experiment.

Results and discussion

Effect of contamination

The secondary electron image quality (IQ), band contrast and sharpness in EBSPs are significantly influenced by the contamination deposited on the specimen surface. This is mainly caused by the interaction between electron beam and residual gases in the Scanning Electron Microscopy (SEM) chamber. Specimen material, preparation, vacuum degree, probe current and exposure time are the main factors contributing to specimen contamination and it is obvious that more residual gas generates more contamination. Figure 1 shows the vacuum degree as a function of time after reaching high vacuum for operation with the applied Field Emission Scanning Electron Microscopy (FESEM). It is strongly recommended to wait for about 50 min after vacuum is ready in order to minimize the contamination. On the other hand, in order to develop an ultra-fast EBSD acquisition technique (Søfferud *et al.*, 2008a) dedicated for real time *in situ* thermo-mechanical observations, high probe current is essential because the maximum speed of pattern

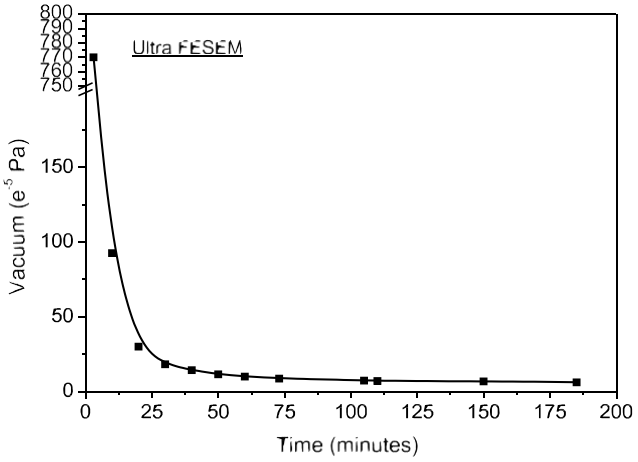

Fig. 1. Vacuum degree as a function of time.

acquisition is proportional to the probe current. Therefore, the effect of contamination has been investigated at high probe currents.

When the beam hits the point from where the EBSP is generated, a contamination layer is built up. The pattern quality is supposed to be strongly influenced by contamination if the step size is smaller than the diameter of the contamination area. Figure 2 shows the indexed points inside the grains in the coarse-grained Ti as a function of step size [probe current 33 nA and frame rate 140 patterns per second (pps)]. The scanned area inside coarse grains depends on the step size and consists of 100 × 100 pixels. It is surprising to observe that the fraction of the indexed points stays constant as the step size decreases from 50 nm to 1 nm. It can be concluded that the fraction of the indexed points in an EBSD map is obviously not influenced by the step size, indicating that contamination is not a problem even at step sizes as small as 1 nm at a

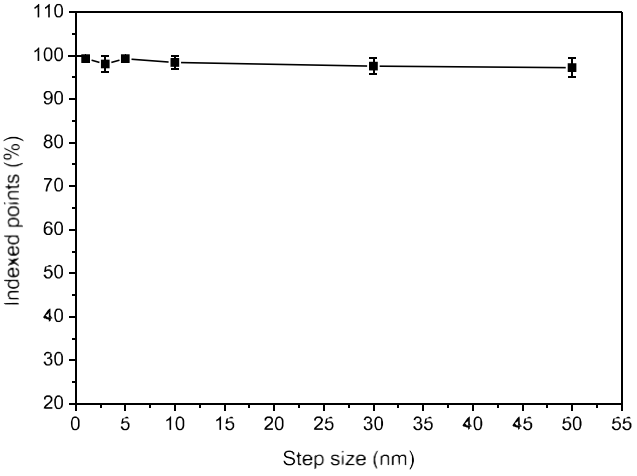

Fig. 2. The indexed points as a function of step size inside coarse grains in coarse-grained Ti.

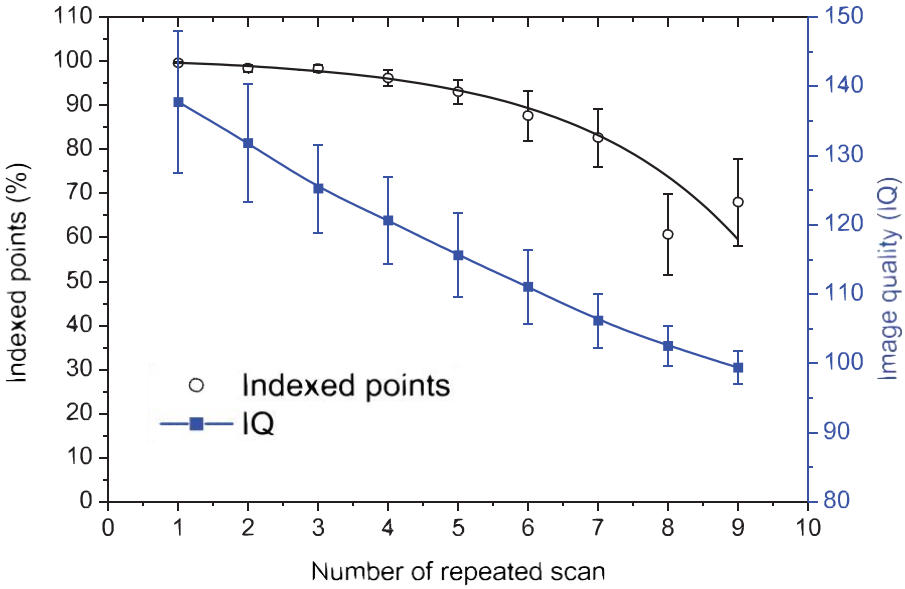

Fig. 3. The effect of number of repeated scan on the indexed points and IQ inside coarse grains in coarse-grained Ti (probe current 33 nA and frame rate 140 pps).

vacuum degree of 6×10^{-5} Pa (the sample is clean and is not mounted). Karlsen (2009) reported a problem related to contamination on a supermartensitic stainless steel when the beam step size was less than 10 nm in a Zeiss Supra 55 VP FESEM. The Zeiss Supra 55 VP and Zeiss Ultra 55 are both available in our laboratory, and it is therefore easy to compare the vacuum performance of these instruments. By comparing the end chamber vacuum it was established that the vacuum in the Zeiss Ultra is about 10 times better than in the Zeiss Supra.

Contamination on a clean and unmounted specimen seems not to be a problem in SEMs with good vacuum even when the step size decreases to 1 nm. This is very advantageous for investigating very fine microstructures in nanostructured/ultrafine-grained materials by EBSD (Fig. 2), where we have to apply a very small step size to image nanoscale grains. *In situ* EBSD observation is a powerful dynamic analytical tool to study fundamental dynamic processes like recovery, recrystallization and the deformation mechanisms, for example grain lattice rotations during plastic deformation. In such experiments repeated scans of the same area are necessary. Therefore, it is of interest to study how contamination builds up during repeated scans and to quantify how this affects the indexing. Figure 3 shows the effect of contamination by repeated scans number on the indexed points and IQ. The fraction of indexed points remains reasonably stable during the first four repetitions and decreases gradually with further repetitions. The IQ seems more sensitive to hydrocarbon contamination and presents almost linear decrease as the number of repeated scan increases from one to nine. This result contrasts with the report of Cocle *et al.* (2007), where the authors observed that hydrocarbon contamination does not significantly influence the average IQ although the EBSP contrast and band sharpness are obviously decreased. The reason may be that higher probe current used in the present study causes more contamination. The evolution of inverse pole figure (IPF) images (3×1 μm^2) and the enlarged images at repeated scan numbers of 1, 5 and 9 are shown in Fig. 4. Figure 4a–c shows the non-indexed points are mainly located at the left edge of

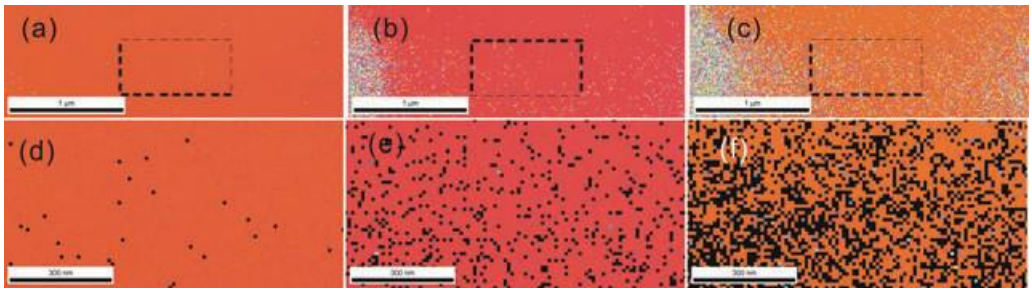

Fig. 4. Evolution of IPF images at repeated scan number of (a) 1, (b) 5 and (c) 9. (d)–(f) are the enlarged images of dotted area in (a)–(c), respectively. The non-indexed points with CI less than 0.08 are highlighted by black.

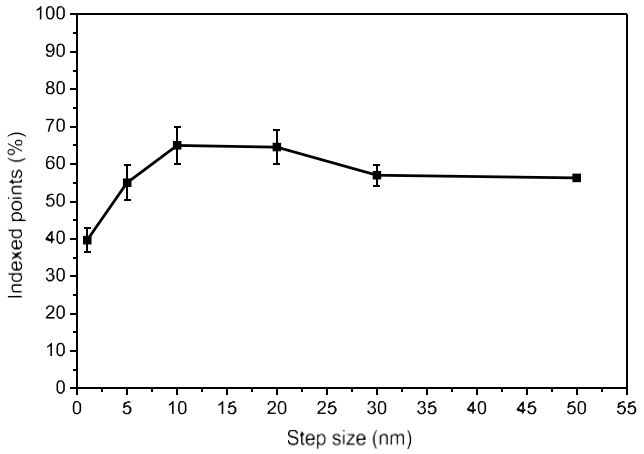

Fig. 5. Indexed points as a function of step size in ultrafine-grained Ti.

the image. In order to eliminate the edge effect, a rectangular dotted area (1 × 0.5 μm^2) was selected from the centre of the original image, as shown in Fig. 4d–f. The colour differences of IPF images in Fig. 4d–f reveal that the orientation changes slightly. Measurement reveals that the orientation slightly changes 2.8° and 3.3° when scan number increases from 1 to 5 and 1 to 9, respectively. This result reveals that the contamination caused by repetitively scanning the same area could lead to artefacts such as orientation changes. The number of non-indexed points increases with increasing repetition number due to increasing contamination layer thickness (seen in Fig. 3).

Effect of step size

Step size is an important EBSD parameter which influences the fraction of indexed points. Figure 5 shows the effect of step size on the indexed points in the ultrafine-grained Ti (probe current 60 nA and frame rate 300 pps). The scan area is 2 × 2 μm^2 in order to contain enough grain boundaries except for the 1 nm step size, where an area of 1 × 1 μm^2 is applied. The fraction of indexed points in ultrafine-grained Ti increases gradually as step size decreases from 50 nm to 10 nm, followed by an obvious decrease as the step size further decreases from 10 nm to 1 nm. It seems that there exists a maximum value of indexed points as a function of step size. By decreasing the step size, the fraction of points in the interior of the grains will increase accordingly. This is why the fraction of indexed points gradually increases as the step size decreases from 50 nm to 10 nm. Matt Nowell (private communication) proposed a method to predict the fraction of non-indexed points (F) based on the fraction of boundary pixels with a hexagonal grid. It can be modified to a square grid set up as following:

$$F = \frac{4D_s}{d}$$

where d is the diameter of the grain assuming a circular grain shape (the same equation can be obtained with a square grain shape) and D_s is the step size. It clearly shows that the predicted fraction of non-indexed points increases as the step size increases at a certain grain size, see simulated line in Fig. 5. This equation can explain the increase of the indexed points when step size decreases from 50 nm to 10 nm. However, this equation does not explain the sharp decrease of the indexed points with further step size reduction (from 10 nm to 1 nm).

In order to reveal the reasons of this issue, IPF maps at step sizes of 20, 10 and 5 nm are shown in Fig. 6. The non-indexed points with CI less than 0.08 are marked by black. Figure 6a–c reveals that the non-indexed points mainly appear on and near the grain boundaries. From these figures it can be seen that the noise at the grain boundaries increases with decreasing step size. It seems that step sizes consisting of a low number of the data acquisition (DAQ) board units generate electronic noise or vibration problems. The DAQ board used in our laboratory has a resolution of 16 bits. The imaging system (DAQ) uses its full dynamic range for scanning the image width at any magnification.

Also coarse-grained Ti samples have been analysed in a similar way as the fine-grained Ti, see Fig. 7. The results from the coarse-grained Ti show the same behaviour as in the fine-grained Ti. In Fig. 8, the fraction of indexed points

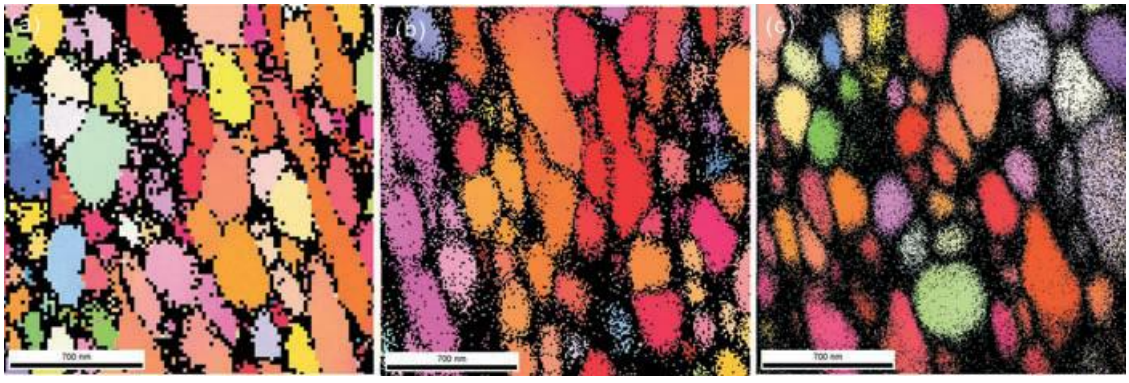

Fig. 6. The IPF images at step sizes of (a) 20 nm, (b) 10 nm and (c) 5 nm in fine-grained Ti. The non-indexed points with CI less than 0.08 are highlighted by black.

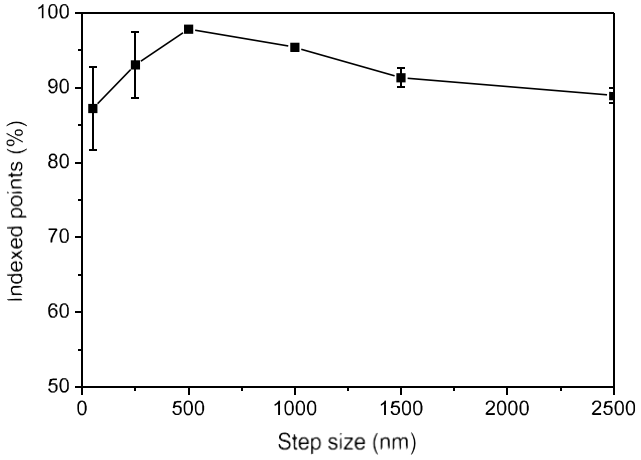

Fig. 7. Indexed points as a function of step size in a coarse-grained Ti sample (probe current 100 nA, frame rate 700 pps and area 100 × 100 μm).

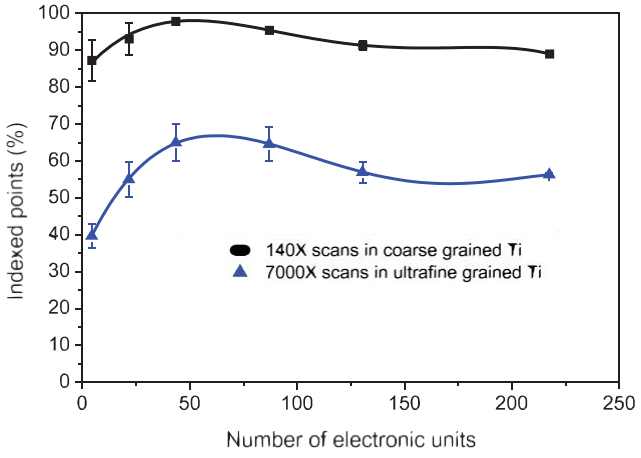

Fig. 8. Summary of indexed points as a function of number of electronic units in both coarse- and fine-grained Ti.

for both coarse- and fine-grained Ti has been plotted as a function of number of electronic units. According to this figure the optimum step size appears at about 50 DAQ board units / electronic step size to get the optimum fraction of indexed points. Figure 8 shows that many non-indexed points are caused by the resolution of the electronic board. The optimum step size (D_o) depends on the magnification (M) and the board resolution / electronic step size can be obtained as follows:

$$D_o = \frac{H_e}{2^{16}} \cdot 50 = \frac{C}{M}$$

where, H_e is the electron image width (micrometres), C is constant depending on the EBSD hardware. In our set up, C is 80 246 (micrometres). Figure 9 shows that the optimum step size as a function of magnification. It shows that the optimum step size decreases sharply at low magnification and decreases slightly with further increasing magnification. This figure is very useful in finding the optimum magnification that can be

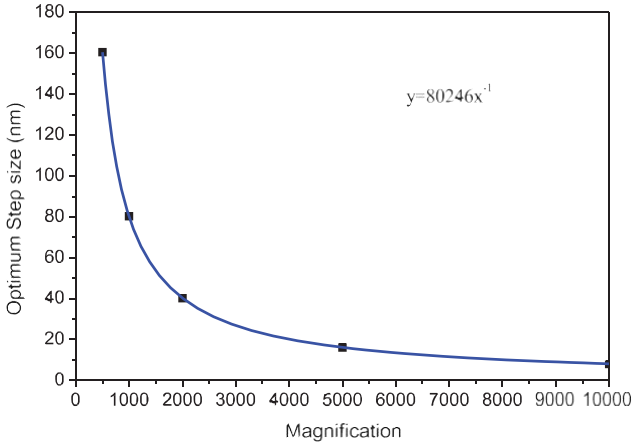

Fig. 9. The optimum step size as a function of magnification.

applied in EBSD mapping. For example, if one decides to use the step size of 100 nm, the optimum magnification should be around 800× according to our DAQ board. Indexing trouble at grain boundaries will occur unless the magnification is about 800×.

Effect of probe current

In order to obtain faster acquisition speed per frame, a higher probe current is needed to maintain the signal to noise ratio because the exposure time is inversely proportional to the acquisition speed. However, the spatial resolution becomes worse by increasing the probe current because the beam size increases correspondingly. Hjelen (1990) and Humphreys (2001) proposed methods to calculate the spatial resolution. However, these methods are not convenient. In this study, a new and easy way to calculate the EBSD resolution is proposed. The effective spatial resolution (R) is defined to be the non-indexed distance perpendicular to the grain boundary, which is given by

$$R = \frac{N_{BP} D_s}{H/D_s} \sin\theta = \frac{N_{BP} D_s^2}{H} \sin\theta$$

where N_{BP} is the number of bad points (CI < 0.08 in this study) at the grain boundary, H is the height of the scan area and θ is the angle between the grain boundaries and the horizon. In this equation, we assume that no topography has been introduced during sample preparation. Figure 10 shows a grain boundary almost perpendicular to the tilt axis, in this example N_{BP} = 83, H = 200 nm, D_s = 5 nm and θ = 80°, the calculated spatial resolution is 10.2 nm. This equation assumes that all non-indexed points are due to overlapping patterns at the grain boundary. The effective resolution perpendicular to the tilt axis is around three times the resolution parallel to tilt axis (Humphreys, 2001). Figure 11 shows the effect of probe current on the effective spatial resolution in a coarse-grained Ti sample (step size 5 nm). It

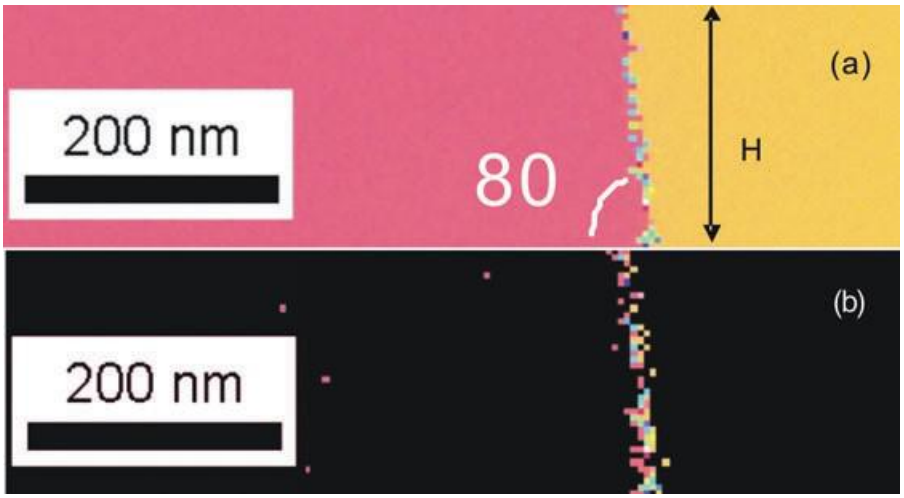

Fig. 10. An example of calculating the effective spatial resolution. (a) IPF map indicates one grain boundary between two grains. (b) Highlight of the non-indexed points with CI less than 0.08

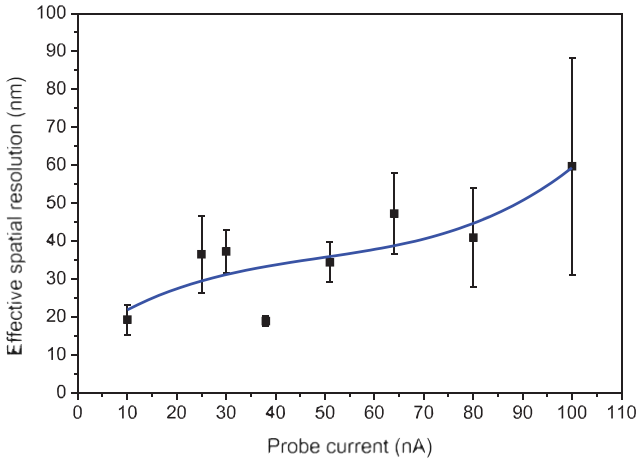

Fig. 11. The effect of probe current on the effective spatial resolution in a coarse-grained pure Ti sample.

seems that the effective spatial resolution tends to increase slightly as the probe current increases from 10nA to 100 nA, which is the same tendency of the resolution of Al (Humphreys, 2001).

To achieve ultra-fast collection speed (frame rate) of EBSD, the camera exposure time (Søfferud *et al.*, 2008a) has to be short and hence the probe current has to be increased (Søfferud *et al.*, 2008b) to maintain the same signal to noise ratio. If we just increase the frame rate without compensating the probe current, the fraction of indexed points and IQ linearly decrease with the increase of frame rate, as shown in Fig. 12. The fraction of the indexed points decreases linearly from 80.7% to 40.4% (Fig. 12a) and the IQ decreases linearly from • to 94.8 (Fig. 12b) when the frame rate increases from 100 to 400 pps at probe current of 30 nA. The acceptable frame rate with reasonable indexed points (56%) seems to be 300 pps at this current. Based on this frame rate, the probe current is reduced with decreasing frame rate at the same ratio, see Fig. 12. The IQ and CI remain reasonably constant (Fig. 12a and b) as frame rate decreases from 300 pps to 50 pps. At larger probe current range, the indexed points slightly decrease when the frame rate increases from 128 to 835 pps by compensating the probe current at the same ratio (Fig. 13). This result is very exciting and can guide further development of the ultra-fast EBSD technique which combines the ultra-fast collection speed and relative good IQ by simply increasing the probe current.

Effect of pattern resolution

Figure 14 shows the indexed points as a function of pattern resolution in coarse-grained Ti sample. The result of a nickel sample (Bjering, 2010) has been cited to compare with the present result. The signal per pixel (exposure time per pixel) keeps constant to make it comparable. The other constant parameters are the probe current (35 nA) and the frame rate (150 pps). The indexed points slightly decrease as pattern resolution decreases from 160 × 160 to 96 × 96, corresponding to binning increase from 3 × 3 to 5 × 5. With further reduction of the pattern resolution, the fraction of indexed points sharply drops. The result suggests that 96 × 96 is the optimum pattern resolution to obtain optimum frame rate and IQ for the applied EBSD system.

Effect of working distance

For a fixed position of EBSD detector, it is well known that the EBSD spatial resolution can be improved by shortening the working distance. However, changing the working distance causes the pattern centre to move up/down on the phosphor screen, and ultimately off the detector screen to the point where there is insufficient EBSP to be automatically indexed (Maitland, 2004). Thus, the size of the phosphor screen and

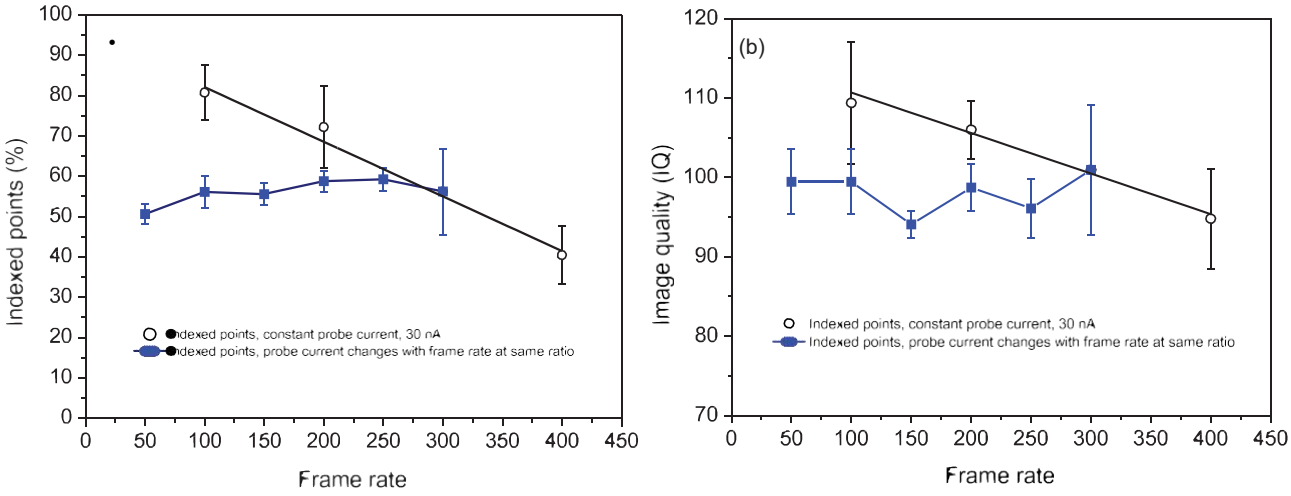

Fig. 12. The effect of frame rate with constant and variable probe current on (a) the indexed points and (b) IQ in a coarse-grained pure Ti sample.

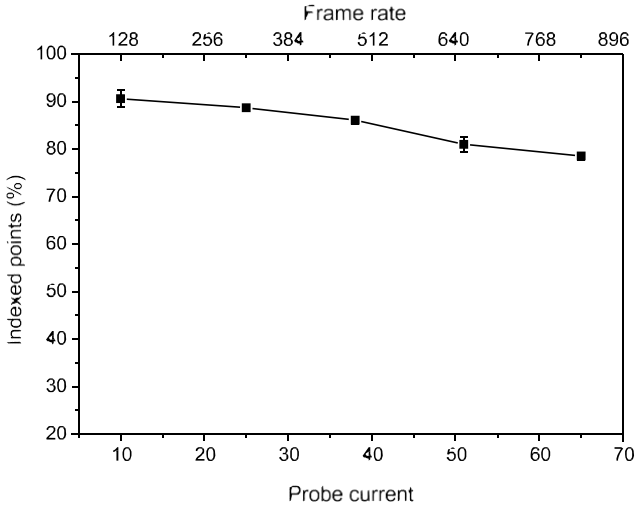

Fig. 13. The effect of probe current and frame rate on the indexed points in a coarse-grained pure Ti sample.

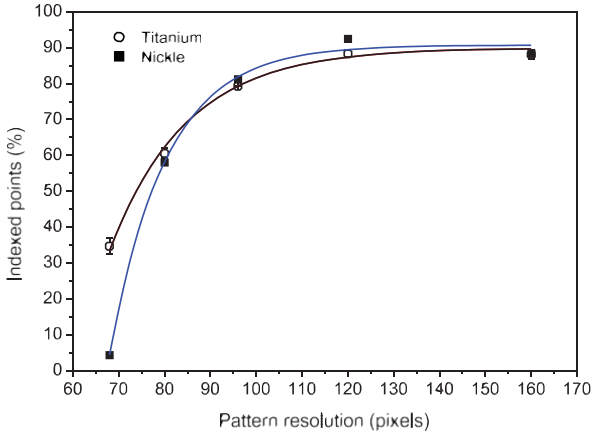

Fig. 14. Indexed points as a function of pattern resolution in coarse-grained pure Ti and nickel.

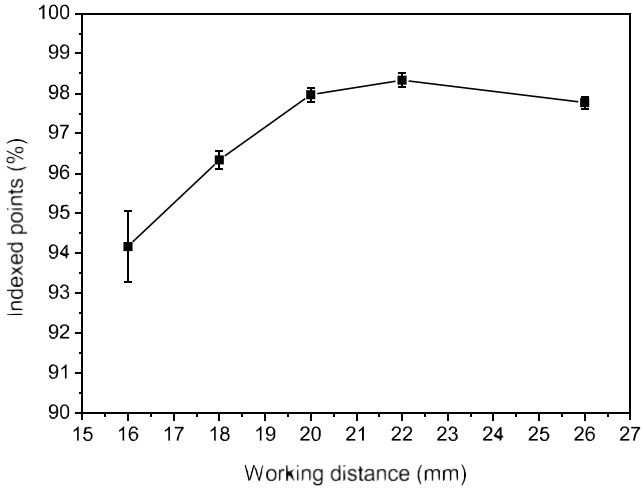

Fig. 15. The effect of working distance on the indexed points in a coarse-grained Ti.

the working distance will influence the fraction of indexed points, as shown in Fig. 15. The optimum working distance of our assembly is around 20–22 mm using a 48-mm-diameter phosphor screen. It is interesting to observe that the fraction of indexed points drops sharply by shortening the working distance and decreases slowly with increasing the working distance. Therefore, improvement of the EBSD spatial resolution by simply decreasing the working distance will significantly sacrifice the indexed points.

Conclusions

The effects of contamination, step size, probe current, pattern resolution and working distance on the fraction of indexed points were investigated and the following results can be concluded based on the present experiments

(1) Contamination on a clean and unmounted specimen is not a problem even when the step size is as small as 1 nm at a vacuum degree of 6×10^{-5} Pa. However, during repeated scans the fraction of indexed points decreases gradually with number of repetitions.
(2) There exists a maximum indexed point peak as a function of step size for both coarse- and fine-grained Ti when the scans include grain boundaries. About 50 DAQ board units are found to be the optimum step size for the applied assembly.
(3) A new and easy method to calculate the effective spatial resolution is proposed. The effective spatial resolution tends to deteriorate slightly as the probe current increases from 10 to 100 nA. The indexed points decrease slightly when the frame rate increases from 128 to 835 pps by compensating the probe current at the same ratio.

109 Based on the applied EBSD hardware and software, the indexed points slightly decrease as pattern resolution decreases from 160 × 160 to 96 × 96 and sharply drop with further decreasing the resolution. The value 96 × 96 is the optimum pattern resolution to obtain optimum frame rate and IQ.

110 For a fixed position of EBSD detector, the fraction of indexed points has a maximum value as a function of working distance and drops sharply by shortening the working distance and decreases slowly with increasing the working distance.

Acknowledgements

The present study was financed by the Norwegian Research Council under the Strategic University Program (192450/I30). We acknowledge Drs. Stuart Wright and Matt Nowell, both at EDAX-TSL, and Dr. François Brisset at CNRS France for valuable comments and corrections.

References

Bjering, O.K. (2010) *In situ EBSD investigation on steel*. Master's Thesis, NTNU, Trondheim, Norway.

Chen, J., Sekiguchi, T., Xie, R., Ahmet, P., Chikyo, T., Yang, D., Ito, S. & Yin, F. (2005) Electron-beam-induced current study of small-angle grain boundaries in multicrystalline silicon. *Scr. Mater*. **52**, 1211–1215.

Chen, Y.J., Li, Y.J., Walmsley, J.C., Dumoulin, S., Skaret, P.C. & Roven, H.J. (2010) Microstructure evolution of commercial pure titanium during equal channel angular pressing. *Mater. Sci. Eng. A.* **527**, 789–796.

Chen, Y.J., Li, Y.J., Walmsley, J.C., Dumoulin, S., Armada, S., Subbarayana, S., Skaret, P.C. & Roven, H.J. (2011) Quantitative analysis of grain subdivision in titanium during equal channel angular pressing. *Scr. Mater*. **64**, 904–907.

Cocle, J., Gauvin, R., Pierre, H., Lagace, M. & Fuerst, C.D. (2007) Evaluation of the SEM-EBSD system stability and hydrocarbon contamination effect on EBSD band contrast response. *Microsc. Microanal*. **13**(Suppl. 2), 946–947.

EDAX/TSL (2007) *OIM Analysis 5.3 Software User Manual*. EDAX/TSL, UT, U.S.A.

Geiss, R., Read, D., Roshko, A., Bertness, K. & Keller, R. (2005) Applications of EBSD to the study of localized deformation. *Microsc. Microanal*. **11**, 516–517.

Hjelen, J. & Nes, E. (1990) Spatial resolution measurements of electron backscatter diffraction patterns (EBSPs) in the scanning electron microscope. *In Proceedings of the XIIth International Congress for Electron Microscopy*. San Francisco, CA, U.S.A. (ed. by L.D. Peachey & D.B. Williams), pp. 404–405.

Humphreys, F.J. (2001) Review grain and subgrain characterisation by electron backscatter diffraction. *J. Mater. Sci*. **36**, 3833–3854.

Karlsen, M. (2009) EBSD based in-situ observations of polycrystalline materials in the SEM. PhD Thesis, Department of Materials Sciences and Technology, NTNU, Trondheim, Norway.

Koblischka-Veneva, A., Müklich, F. & Koblischka, M.R. (2002) A study of grain orientation of Alkali doped polycrystalline YBCO ceramics using an EBSD technique. *Cryst. Eng*. **5**, 411–418.

Krieger Lassen, N.C., Conradsen, K. & Juul Jensen, D. (1992) Image processing procedures for analysis of electron diffraction patterns. *Scanning Microsc*. **6**, 115–121.

Magdalena, L.P. (2003) The effectiveness of automated electron backscatter diffraction in the analysis of rock-forming minerals and metals. Master Thesis, University of Liverpool, Liverpool.

Maitland, T. (2004) EBSD – current achievements in speed and resolution. *Microsc. Microanal*. **10**, 936–937.

Nowell, M.M., Farrer, J.K. & Witt, R.A. (2003) The effects of EBSD collection speed on indexing accuracy. *Microsc. Microanal*. **9**, 722–723.

Pantleon, W. (2008) Resolving the geometrically necessary dislocation content by conventional electron backscattering diffraction. *Scr. Mater*. **58**, 994–997.

Saxl, I., Kalousov, A., Ilucov, L. & Sklenicka, V. (2009) Grain and subgrain boundaries in ultrafine-grained materials. *Mater. Charact*. **60**, 1163–1167.

Schwartz, A.J., Kumar, M. & Adams, B.L. (2000) *Electron Backscatter Diffraction in Materials Science*. Kluwer Academic/Plenum Publishers, New York.

Schwarzer, R.A. & Hjelen, J. (2010) High-speed orientation microscopy with offline solving sequences of EBSD patterns. *Solid State Phenom*. **160**, 295–300.

Søfferud, M., Hjelen, J., Karlsen, M., Dingley, D. & Jaksch, H. (2008a) Future prospects on EBSD speeds using a 40 nA FESEM: *EMC 2008 In 14th European Microscopy Congress* 1–5 *September 2008, Aachen, Germany* (ed. by M. Luysberg, K. Tillmann & T. Weirich). Springer, Berlin, pp. 625–626.

Søfferud, M., Hjelen, J., Karlsen, M., Breivik, T., Krieger Lassen, N.C. & Schwarzer, R. (2008b) Development of an ultra-fast EBSD detector system: *EMC 2008 In 14th European Microscopy Congress* 1–5 *September 2008, Aachen, Germany* (ed. by M. Luysberg, K. Tillmann & T. Weirich). Springer, Berlin, pp. 623–624.

Valiev, R.Z., Islamgaliev, R.K. & Alexandrov, I.V. (2000) Bulk nanostructured materials from severe plastic deformation. *Prog. Mater. Sci*. **45**, 103–189.

Venables, J.A. & Harland, C.J. (1973) Electron back scattering patterns – new technique for obtaining crystallographic information in the scanning electron microscope. *Phil.Mag*. **27**, 1193–1200.

Wright, S. & Nowell, M. (2008) High-speed EBSD. *Adv. Mater. Process*. **166**, 29–31.

Wright, S.I., Nowell, M.M. & Field, D.P. (2011) A review of strain analysis using electron backscatter diffraction. *Microsc Microanal*. **17**, 316–329.